Rutherford backscattering analysis of porous thin TiO_2 films

M. Mayer [a] U. von Toussaint [a] J. Dewalque [b] O. Dubreuil [b]
C. Henrist [b] R. Cloots [b] F. Mathis [c]

[a] *Max-Planck-Institut für Plasmaphysik, EURATOM Association, Boltzmannstr. 2, 85748 Garching, Germany*

[b] *University of Liege, Department of Chemistry, GreenMat-LCIS, B6a Sart Tilman, 3 Alle de la Chimie, 4000 Lige, Belgium*

[c] *Universit of Lige - FNRS, Centre Europen d'Archomtrie - IPNAS, B5, Sart Tilman, 10 Alle du 6 aout, 4000 Lige, Belgium*

Abstract

The additional energy spread due to sample porosity was implemented in the SIMNRA simulation code, version 6.60 and higher. Deviations of the path length and energy loss distributions from the ones expected from a Poisson distribution of the number of traversed pores are taken into account. These deviations are due to the interaction of pores at higher pore concentrations by overlap or blocking. The skewnesses of the energy distributions are approximated by two-piece normal distributions with identical first three moments. Propagation of porosity-induced energy spread in thick layers is taken into account. Calculated results are compared to experimental data obtained with thin TiO_2 mesoporous films measured by Rutherford backscattering (RBS),transmission electron microscopy (TEM), and atmospheric poroellipsometry.

Key words: Computer software, Data analysis, Simulation, Ion beam analysis, Porous Materials

1 Introduction

Ion beam analysis (IBA) techniques detecting energy spectra of charged particles, such as Rutherford backscattering (RBS), elastic recoil detection analysis (ERDA) and nuclear reaction analysis (NRA), are usually considered as methods for the quantitative determination of depth profiles of elements in thin films [1,2]. For laterally inhomogeneous samples IBA energy spectra yield additional information about the lateral distribution of material in the sample

Article published in Nucl. Instr. Meth. B 273 (2012) 83

[3]. The analysis of inhomogeneous materials containing pores or inclusions has gathered interest since many years. As has been already shown in [4–7], the presence of randomly distributed hollow pores results in an additional energy broadening for incident and exit beams. This additional energy broadening contains information about the volume fraction of pores and their diameters, so that this information can be extracted from IBA energy spectra. But even in cases when the properties of a porous layer are not of primary interest, the additional energy spread due to porosity has to be properly implemented in simulation codes, as otherwise differences between a measured and a simulated spectrum will occur: This can hamper the successful evaluation of spectra from such types of samples.

Stoquert and Szörényi [6] developed a model which allows to calculate the additional energy spread induced by sample porosity using the following assumptions:

(1) Pores are randomly distributed without long- or short range order.
(2) The number of pores traversed by the incident and outgoing ion beams is assumed to be Gaussian: If the beam traverses some path length in the material and traverses in mean N pores, then the distribution of the actual number of traversed pores has a standard deviation $\sqrt{N}$. This is a special case for larger N of the assumption of a Poisson distribution for the number of traversed inclusions.
(3) The energy spread distribution is assumed to be Gaussian.
(4) The effective stopping power S_{eff} is assumed to be constant.
(5) Propagation of porosity-induced straggling in thicker layers is neglected.

However, as was shown by Mayer and v. Toussaint [8], the Stoquert/Szörényi model is oversimplified:

(1) The assumption of a Poisson (or Gaussian) distribution for the number of traversed pores is only valid for sparse, non-interacting pores. This is only correct for small volume fractions of pores below about 5 vol%. At higher volume fractions the probability for interaction between pores increases and cannot be neglected, where the interaction between pores is either overlap (if overlap of pores is allowed) or blocking (in the case of non-overlapping pores). This interaction was modeled by Monte-Carlo simulations of pore distributions [8] and results in deviations from the results expected from Poisson distributions, with the variance of the path length distribution function considerably smaller than expected from Poisson. The Stoquert/Szörényi model therefore overestimates the width of porosity-induced straggling at pore volume fractions above about 5%.
(2) The path length distributions and the corresponding energy distributions of slowing-down particles have non-Gaussian shapes with usually non-vanishing third moments and skewnesses. The energy distributions have

a strongly non-Gaussian shape close to the surface of the porous layer. With increasing depth the distributions slowly converge towards Gaussian distributions. However, the initial skewness vanishes only slowly, so that the Gaussian limit is reached only at large depths. The skewness is very small at pore volume fraction of about 40%.

(3) For thicker porous layers the assumption of a constant stopping power S_{eff} gets invalid. In addition non-stochastic propagation of straggling due to the shape of the stopping power has to be taken into account. This effect is similar to non-stochastic propagation of electronic energy-loss straggling [9] and can be treated using similar methods. This was already shortly sketched in [8].

This paper describes the implementation details of the theory presented in [8] in the code SIMNRA 6.60 and higher. Problems arising due to the non-Gaussian shape of the distributions are discussed. Simulation calculations are compared to experimental data obtained from mesoporous TiO_2 thin films with pore diameters of a few nm, pore volume fraction in the range 20–40 vol.% and film thicknesses in the range 100–300 nm. The films were deposited on silicon substrates [10,11]. These mesoporous anatase thin films are a promising materials to act as electrodes in dye-sensitized solar cells (DSSC's). The microstructural properties of the films were characterised by X-ray diffraction (XRD), transmission electron microscopy (TEM) and atmospheric poroellipsometry (AEP).

2 Experimental

Film were deposited using Pluronic surfactant as template. Two precursor solutions were used: The first one (called F127 solution) was composed by ethanol (Sigma Aldrich), Pluronic F127 ($EO_{106}PO_{70}EO_{106}$, Sigma Aldrich), titanium tetraisopropoxide (Acros Organics) and concentrated hydrochloric acid (Merck, 36 wt.%). The second solution (P123 solution), was prepared by mixing 1-butanol (Acros Organics), Pluronic P123 ($EO_{20}PO_{70}EO_{20}$, Sigma Aldrich), titanium tetraisopropoxide (Acros Organics) and concentrated hydrochloric acid (Merck, 36 wt.%). Films were dip-coated on silicon substrates. To study the influence of the film organization on the porosity, two different relative humidity (RH) conditions were applied during the film synthesis process to tune the mesostructure. Isotropic mesoporous films, known as worm-like, were obtained at a RH of 25–30% [11]. The withdrawal rate was fixed at 5 mm/s for the F127 solution (film thickness ≈200 nm) and at 0.8 mm/s for the P123 solution (film thickness ≈350 nm). To obtain anisotropic ordered films, known as gridlike, the RH in the dip-coating chamber was set at 25–30% at 25°C and the as-obtained films were directly transferred into an ageing chamber under controlled humidity of 75% during one day. The withdrawal

rate was 1.5 mm/s for the F127 solution (film thickness ≈100 nm) and at 0.8 mm/s for the P123 solution (film thickness ≈350 nm).

TEM micrographs were taken at an acceleration voltage of 200 kV (Tecnai G2 Twin, FEI) on films scratched off the substrate and dispersed in ethanol under ultrasound, then deposited on carbon-coated copper grids. Ellipsometry measurements were performed on a UV-visible (from 250 nm to 1000 nm) GES5E Spectroscopic Ellipsometer from SOPRALAB, the data analysis was performed with the WINSE software. The ellipsometer was coupled with an ellipsometric porosimetry device for atmospheric poroellipsometric measurements [12]. This device consists of a chamber containing the film to analyze. The environment of the film is modulated by a pulsed air flow with controlled partial pressure of water. Measurement of the adsorption-desorption hysteresis of the water into the film porosity allows the determination of the percentage of porosity and the surface area. A pore size distribution (PSD) can be calculated from the AEP data.

Rutherford backscattering (RBS) measurements were performed using 1 and 2 MeV ^{4}He ions at a scattering angle of 155° at normal incidence at the IPNAS-CEA Laboratory of Liège. The detector resolution was 11 keV FWHM, the energy spread of the incident beam was about 5 keV FWHM. The measurement was made in vacuum at a background pressure of about 10^{-6} mbar.

3 Computer simulation

The additional energy spread induced by porosity was implemented in SIMNRA 6.60 [13] using the results from [8]. This reference presents the first three moments of the path length distribution function for randomly distributed, overlapping spherical pores in three dimensions. The length L of the cubical unit cell is given by

$$c_V = \frac{4\pi}{3}\frac{R^3}{L^3}, \tag{1}$$

with c_V the volume fraction of pores and R the radius of the pores. All pores are assumed to have identical radius.

SIMNRA approximates the typically skewed energy distributions by two-piece normal distributions (TPND) (sometimes called binormal distribution

or joined half-Gaussian) $f(x)$ given by

$$f(x) = \begin{cases} A \exp\left(-\frac{(x-x_0)^2}{2\sigma_1^2}\right) \text{ if } x \leq x_0 \\ \\ A \exp\left(-\frac{(x-x_0)^2}{2\sigma_2^2}\right) \text{ if } x > x_0 \end{cases} \tag{2}$$

x_0 is the mode of the distribution, σ_1 and σ_2 are the standard deviations towards lower and higher values. A is a normalization factor.

The TPND allows to adjust mean value F, variance V and third central moment M. For not too strongly skewed distributions and given F, V and M the parameters are obtained from

$$\sigma_1 = -\frac{\beta}{2} + \sqrt{\frac{\beta^2}{4} - a\beta^2 + V} \tag{3}$$

$$\sigma_2 = \frac{\beta}{2} + \sqrt{\frac{\beta^2}{4} - a\beta^2 + V} \tag{4}$$

$$x_0 = F - \frac{M}{V} \tag{5}$$

with the abbreviations

$$a = 1 - \frac{2}{\pi} \approx 0.3634 \tag{6}$$

and

$$\beta = \sqrt{\frac{\pi}{2}}\frac{M}{V}. \tag{7}$$

For thick porous layers non-stochastic propagation of straggling due to the shape of the stopping power plays an important role and has to be taken into account. If an energy-distributed beam with initial variance V_i penetrates a layer with thickness Δx, then the variance of the energy distribution after the layer is given by [9] (see also [14]):

$$V_f = \left(\frac{S_f}{S_i}\right)^2 V_i + G\Delta x, \tag{8}$$

with S_i the stopping power at the entrance and S_f the stopping power at the exit of the layer. G is the porosity-induced variance of straggling per unit length. Eq. 8 is identical to the case of electronic energy-loss straggling [9],

but with a different G. However, eq. 8 is only strictly accurate for infinitesimally small Δx. It gets more and more inaccurate for larger Δx, because the propagation of straggling for the second term in eq. 8 is neglected. Small step widths Δx therefore increase the accuracy of straggling calculations, but also increase the computing time. Therefore, a reasonable compromise for an automatic determination of the step width Δx has to be found which balances both accuracy and computing time.

The error ΔV_f of V_f (see eq. 8) can be estimated to be

$$\Delta V_f \leq \begin{cases} \left|1 - \left(\frac{S_f}{S_i}\right)^2\right| G\Delta x \text{ if } |(1 - S_f/S_i)^2| > 0.03 \\ 0.03\, G\Delta x \qquad\qquad \text{else.} \end{cases} \tag{9}$$

The factor 0.03 in the bottom half of eq. 9 is based on extensive tests: Using only the upper half of the equation results in unrealistically small error estimates (and too large step widths, if the error estimate is used for a step width control) in the vicinity of the stopping power maximum, where $S_f \approx S_i$ on both sides of the maximum.

The step width Δx for straggling calculations is selected in such a way, that

$$\frac{\Delta V_f}{V_f} \leq \delta, \tag{10}$$

where δ is the desired accuracy. SIMNRA uses a default of $\delta = 1\%$. The estimated accuracy of all straggling calculations can be inspected with the program VIEWNRA, which is part of the SIMNRA package.

As example for the propagation of straggling the straggling contributions of a 5 MeV proton beam penetration porous carbon with 30% porosity fraction and different pore diameters is shown in Fig. 1. At small energy losses the propagation of straggling plays only a minor role, and the widths of the straggling contributions by energy-loss straggling and sample porosity increase approximately as $\sqrt{x}$, where x is the depth in the sample. At larger energy losses the widths of the straggling contributions get dominated by non-stochastic propagation due to the characteristics of the stopping power, resulting in a steeper increase of the straggling widths. For small pores with diameters below about 200 nm the energy spread due to energy-loss straggling plays the dominant role, while for larger pore diameters the energy spread induced by porosity becomes the dominant contribution.

The propagation of the straggling asymmetry can be computed with the methods outlined in [15], using the third moment of the porosity-induced straggling from [8]. It is noteworthy that for porosity fractions below about 40 vol.%

the skewness of the path length distribution inside pores is positive. This means for hollow pores without stopping power, that the energy distributions of particles slowing-down in a porous layer have a positive skew at low pore concentrations. This is at least uncommon, because other energy spread contributions (due to energy-loss straggling or multiple scattering) always have a negative skewness. At a porosity volume fraction of about 40% the third central moment gets zero, so that porosity-induced energy distributions are almost symmetrical. At volume fractions above 40% the skewness finally gets negative.

As already discussed in [8], the path length distributions and the corresponding energy distributions are strongly non-Gaussian for small path lengths in the porous layer, i.e. close to the surface of the porous layer. It requires typically 5–10 traversed pores before the distribution can be described with sufficient accuracy by a TPND, and typically more than 20 pores before it can be approximated by a Gaussian. Moreover, for small path lengths correlations between incident and exit paths (which are neglected) play a larger role. The model therefore yields meaningful results only, if the porous layer exceeds some minimum layer thickness: The beam should traverse at least about 5 pores. Moreover, the approximation of the path length distribution by a TPND (or Gaussian) at small path lengths may result in a (typically small) shift of the high energy edge of an RBS spectrum towards higher energies: This is due to the steeper increase of the width of the porosity-induced straggling $\propto \sqrt{x}$, with x the depth inside the porous layer, than the energy loss, which increases $\propto x$: For small values of x the width of the distribution always exceeds the mean energy loss. This distortion of the high-energy edge could be only avoided by using the correct path length distribution function. However, because this function cannot be convoluted analytically, this would require an additional numerical convolution, which is very costly in terms of computing time. As this does not provide any new information but only avoids a typically small distortion of the spectrum, this is not worth the effort. But it should be kept in mind that the high-energy edge of a simulated spectrum from a porous layer should not be interpreted.

The shape of sharp resonances (such as the well known 3.05 MeV resonance for α-particles scattered from ^{16}O) is not calculated correctly by SIMNRA 6.60, because the necessary double-integral from [7] is not implemented.

4 Results and discussion

The porosity of the deposited TiO_2 films was examined in [11,12] by transmission electron microscopy (TEM) and by atmospheric poroellipsometry (AEP). The pores were arranged in two different types of structures, depending on de-

position conditions [11]: Samples deposited under 25% relative humidity (RH) and directly stabilized at 300°C show an isotropic, random distribution of pores, referred to as "wormlike" structure. In this structure pores and walls are interpenetrated. Films deposited under 25% RH and aged at 75% RH before stabilization have an oriented long-range order known as "gridlike" mesostructure. Because the model from [8] is valid for random distributions of pores, it can be applied to the "wormlike" structures. Application to the "gridlike" structures is more problematic due to the oriented, non-random arrangement of pores. The "gridlike" structures will be not treated here.

The pore size distributions were calculated from the AEP data using a model assuming cylindrical pores closed on one end. The pore size distributions could be fitted with two Gaussian functions having mean pore diameters of 6.6 and 7.6 nm. The widths of both Gaussian distributions were about 2 nm FWHM [12]. However, due to the somewhat unrealistic model of cylindrical pores these numbers should be treated with some care. The pore diameter visible in the TEM micrographs was in the range 7–10 nm, but it is difficult to get statistically sound results from the TEM images. Moreover, the TEM images were obtained from film scratched from the substrates, which may result in distortions. Assuming spherical pore shapes, the measured porosity fractions and internal surface areas from [11, Table 2] allow to estimate the pore diameter to be in the range 9–12 nm.

The different energy spread contributions are shown in Fig. 2 as a function of TiO_2 depth. For layer thicknesses below about 50 nm the total energy spread is dominated by the finite energy resolution of the detector, while for layer thicknesses above about 50 nm the energy spread due to layer porosity gets the main contribution to the total energy spread: A measurement of the energy spread therefore allows to derive information about the porosity.

An experimental RBS spectrum with 1 MeV incident ^{4}He ions is shown in Fig. 3. The layer thickness from RBS was 1.32×10^{18} atoms/cm^2, while ellipsometry gave a thickness of 240 nm. This yields a density of 5.5×10^{22} atoms/cm^3. Assuming that the anatase matrix material between the pores has the theoretical density of 8.8×10^{22} atoms/cm^3, this gives a porosity fraction of 37.5%: This is in good agreement with the value measured by poroellipsometry of 34.5%.

In general, the width of the pore-induced energy spread depends on pore volume fraction and pore diameter. However, at pore volume fractions in the range 30–40% the width of the pore-induced energy spread gets almost independent of pore volume fraction [8, Fig. 6], so that a measurement of the energy straggling basically measures the pore diameter. The low-energy edge of the Ti-peak (in channels 1050–1150) is considerably broader than the simulation assuming a dense, non-porous and smooth layer (dashed line in Fig. 3).

The experimental data can be simulated assuming a pore diameter of 11 nm (Fig. 3 solid line), which is in good agreement with the data obtained by AEP and TEM, keeping the uncertainties of all methods in mind. The RBS-value for the mean diameter may be slightly too large due to the distribution of pore sizes: This adds an additional variance, which is not taken into account by the model of equally-sized pores in [8].

5 Conclusions

The first three moments of the path length distribution function and of the corresponding energy distributions were derived by Monte-Carlo simulations for spherical pores in three dimensions [8]. For pore concentrations larger than about 5 vol.% the width of the pore-induced energy spread is considerably smaller than expected from a Poisson distribution for the number of pores in each volume. The energy spread distributions generally converge only slowly towards Gaussian distributions due to the initial skewness of the distributions. The results from [8] were implemented in the SIMNRA code, version 6.60 and higher. The skewness of the energy distributions is taken into account by the third central moment and by an approximation of the energy distributions by two-piece normal distributions. Propagation of pore-induced energy spread in thick layers is taken into account in analogy to the propagation of energy-loss straggling. An automatic step-width control allows to achieve a defined accuracy of straggling calculations.

Simulated results were compared to experimental RBS spectra of porous TiO_2 layers with pore volume fractions of 20–40%. Analysis of the measured RBS spectra gives pore diameters of about 11 nm. This is in reasonable agreement with results obtained by atmospheric poroellipsometry, transmission electron microscopy and internal surface area [11,12], which gave pore diameters in the range 7–12 nm. RBS of thin porous layers therefore offers the possibility to derive information about the diameter of pores in these layers.

References

[1] J.R. Tesmer and M. Nastasi, Eds. *Handbook of Modern Ion Beam Materials Analysis*, first ed. Materials Research Society, Pittsburgh, Pennsylvania, 1995.

[2] Y. Wang and M. Nastasi, Eds. *Handbook of Modern Ion Beam Materials Analysis*, second ed. Materials Research Society, Warrendale, Pennsylvania, 2009.

[3] M. Mayer, W. Eckstein, H. Langhuth, F. Schiettekatte, and U. von Toussaint. Nucl. Instr. Meth. B (2011) . in print.

[4] B.H. Armitage, J.D.F. Ramsay, and F.P. Brady. Nucl. Instr. Meth. 149 (1978) 329.

[5] G. Amsel, E. d'Artemare, G. Battistig, V. Morazzani, and C. Ortega. Nucl. Instr. Meth. B 122 (1997) 99.

[6] J.P. Stoquert and T. Szörényi. Phys. Rev. B66 (2002) 144108.

[7] M. Tosaki. J. Appl. Phys. 99 (2006) 034905.

[8] M. Mayer and U. von Toussaint. Nucl. Instr. Meth. B (2011) . submitted.

[9] E. Szilágyi, F. Pászti, and G. Amsel. Nucl. Instr. Meth. B 100 (1995) 103.

[10] C. Henrist, J. Dewalque, F. Mathis, and R. Cloots. Microporous and Mesoporous Materials 117 (2009) 292.

[11] J. Dewalque, R. Cloots, F. Mathis, O. Dubreuil, N. Krins, and C. Henrist. J. Mater. Chem. (2011) . in print.

[12] O. Dubreuil, J. Dewalque, G. Chêne, F. Mathis, G. Spronck, D. Strivay, R. Cloots, and C. Henrist. Microporous and Mesoporous Materials (2011) . submitted.

[13] M. Mayer. SIMNRA user's guide. Tech. Rep. IPP 9/113, Max-Planck-Institut für Plasmaphysik, Garching, 1997.

[14] D.K. Brice. Thin Solid Films 19 (1973) 121.

[15] M. Mayer, K. Arstila, and U. von Toussaint. Nucl. Instr. Meth. B 268 (2010) 1744.

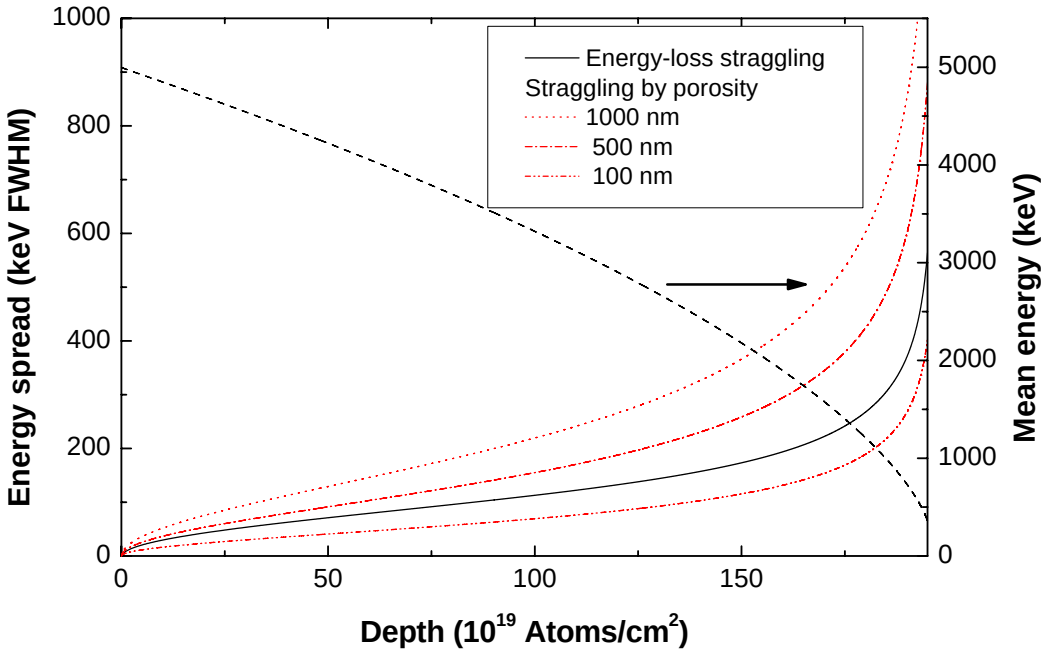

Fig. 1. Energy straggling of 5 MeV protons in carbon with 30% porosity fraction for pore diameters of 1000 nm, 500 nm and 100 nm. Dashed line: Mean energy of the particle beam; Solid line: Width of the energy spread distributions due to energy-loss straggling; Dotted and dash-dotted lines: Widths of the energy spread distributions due to sample porosity for different pore diameters.

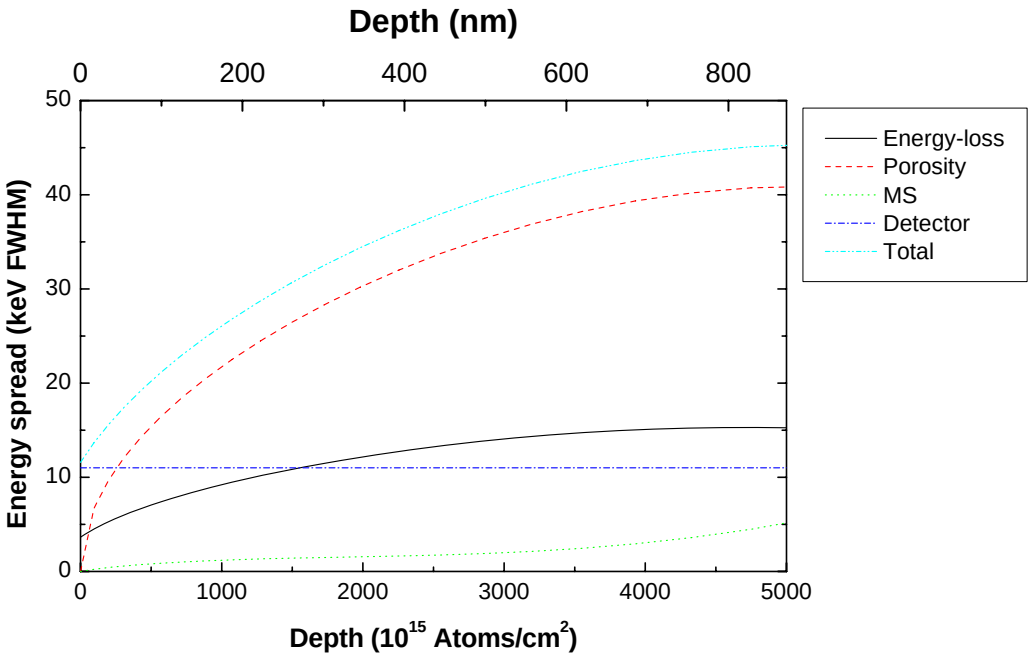

Fig. 2. Energy spread contributions for 1 MeV ^{4}He in porous TiO_2 (volume fraction of pores 35%, pore diameter 11 nm), backscattered from ^{48}Ti at a scattering angle of 155°. Energy spread of incident beam 5 keV. Solid line: Energy-loss straggling, including energy spread of incident beam; Dashed line: Energy spread due to porosity; Dotted line: Energy spread due to multiple small-angle scattering; Dash-dotted line: Detector resolution; Dash-dot-dotted line: All contributions. A mass density of 2.54 g/cm^3 was used for the porous material.

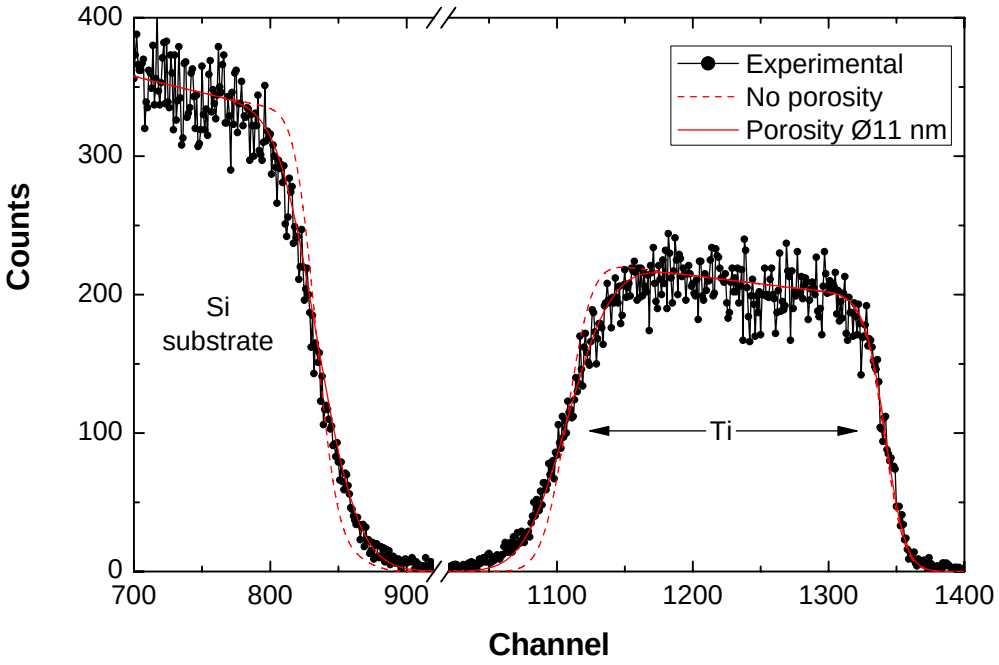

Fig. 3. RBS spectrum of a porous TiO_2 layer on Si, measured with 1 MeV ^{4}He. F127, wormlike. Dots: Experimental data; Dashed line: Computer simulation using SIMNRA 6.60 assuming a dense layer without porosity; solid line: Simulation assuming a porous layer with 11 nm pore diameter.